Redox Biology 54 (2022) 102382

Contents lists available at ScienceDirect

Redox Biology

journal homepage: www.elsevier.com/locate/redox

Farnesoid X receptor protects against cisplatin-induced acute kidney injury by regulating the transcription of ferroptosis-related genes

Dong-Hyun Kim, Hoon-In Choi, Jung Sun Park, Chang Seong Kim, Eun Hui Bae, Seong Kwon Ma, Soo Wan Kim *

Department of Internal Medicine, Chonnam National University Medical School, Gwangju, 61469, South Korea

ARTICLE INFO

Keywords:
Farnesoid X receptor (FXR)
Ferroptosis
Acute kidney injury (AKI)
Reactive oxidative stress (ROS)
MAF bZIP transcription factor G (MAFG)

ABSTRACT

The side effects of cisplatin, a widely used chemotherapeutic agent, include nephrotoxicity. Previous studies have reported that cisplatin induces ferroptosis and lipid peroxide accumulation. Ferroptosis, a type of regulated cell death, is characterized by iron-dependent lipid peroxidation. Although previous studies have examined the regulation of ferroptosis in acute kidney injury (AKI), the regulatory mechanism of ferroptosis has not been elucidated. Here, the ability of activated farnesoid X receptor (FXR) to attenuate cisplatin-induced AKI through the regulation of ferroptosis was examined. FXR deficiency exhibited more ferroptosis responses, such as increase in lipid peroxidation, iron content and heme oxygenase 1 protein, and a decrease in glutathione/glutathione disulfide ratio and glutathione peroxidase 4 levels in HK2 cells and mice. Increased blood urea nitrogen, serum creatinine, and ferroptotic responses in the cisplatin-induced AKI mouse model were mitigated upon treatment with the FXR agonist GW4064 but were exacerbated in FXR knockout mice. RNA sequencing analysis revealed that ferroptosis-associated genes were novel targets of FXR. FXR agonist upregulated the expression of lipid and glutathione metabolism-related genes and downregulated cell death-related genes. Additionally, chromatin immunoprecipitation assays, using mice renal tissues, revealed that agonist-activated FXR could bind to its known target genes (*Slc51a*, *Slc51b*, *Osgin1*, and *Mafg*) and ferroptosis-related genes (*Aifm2*, *Ggt6*, and *Gsta4*). Furthermore, activated FXR-dependent MAFG, a transcriptional repressor, could bind to *Hmox1*, *Nqo1*, and *Tf* in the renal tissues of FXR agonist-treated mice. These findings indicate that activated FXR regulates the transcription of ferroptosis-related genes and protects against cisplatin-induced AKI.

1. Introduction

Acute kidney injury (AKI), a common clinical condition among hospitalized patients, is associated with increased morbidity and mortality. AKI occurs in 5–10% of all hospitalized patients and increases the risk of developing chronic kidney disease (CKD) and end stage renal disease [1,2]. Cisplatin is a widely used therapeutic agent for solid organ cancer; however, its the side effects include nephrotoxicity. The incidence of AKI among patients undergoing cisplatin therapy is 30%. Hence, cisplatin treatment must be suspended in these patients as there are no approved therapeutics for AKI [3,4]. Although the mechanism underlying cisplatin-induced AKI has not been completely elucidated, it may be related to associated cell death-related pathologies, such as apoptosis, autophagy, oxidative stress, and inflammation [5]. Recent studies have examined the therapeutic effect of inhibiting ferroptosis, a type of cell death, in cisplatin-induced AKI. However, the mechanism underlying ferroptosis regulation has not been elucidated.

Ferroptosis is a type of non-apoptotic regulated cell death caused by iron-dependent accumulation of lipid hydroperoxide [6]. Previous studies have reported that ferroptosis is associated with the pathogenesis of several diseases, such as cancer, stroke, neurodegenerative disorders, acute myeloid leukemia, liver fibrosis, and ischemia/reperfusion (I/R) kidney injury [7,8]. The metabolic pathways of lipid, iron, and amino acids are closely correlated with ferroptosis. Several genes, including *Hmox1*, *Acsl4*, *Gpx4*, and *Slc7a11*, and chemical compounds and drugs, including erastin, RSL3, ferrostatin-1, peroxidation inhibitors, and antioxidants, are reported to regulate ferroptosis [7,9].

Nuclear receptors (NRs), which are ligand-regulated or hormone-regulated transcriptional factors, are involved in physiological and pathological processes [10]. Farnesoid X receptor (FXR, also known as NR1H4), a member of the NR family, exerts nephroprotective effects in several diseases, including obesity, diabetes, aging, AKI, and CKD [11–15]. Additionally, FXR plays a key role in maintaining cholesterol

* Corresponding author. Department of Internal Medicine, Chonnam National University Medical School, 42 Jebongro, Gwangju, 61469, South Korea.
E-mail address: skimw@chonnam.ac.kr (S.W. Kim).

https://doi.org/10.1016/j.redox.2022.102382
Received 7 June 2022; Accepted 20 June 2022
Available online 23 June 2022

Abbreviations

FXR	Farnesoid X Receptor
AKI	Acute Kidney Injury
GPX4	Glutathione Peroxidase 4
ROS	Reactive Oxidative Stress
GSH/GSSG ratio	Reduced Glutathione/Oxidized Glutathione ratio
AIFM2 (FSP1)	Apoptosis Inducing Factor Mitochondria Associated 2 (ferroptosis suppressor protein 1)
GGT6	Gamma-Glutamyltransferase 6
GSTP1	Glutathione S-transferases P1
GSTP2	Glutathione S-transferases P2
GSTA3	Glutathione S-Transferase Alpha 3
Gsta4	Glutathione S-Transferase Alpha 4
SLC51a	Solute Carrier Family 51, alpha subunit
SLC51b	Solute Carrier Family 51, beta subunit
OSGIN1	Oxidative Stress Induced Growth Inhibitor 1
MAFG	MAF BZIP Transcription Factor G
HMOX1	Heme Oxygenase 1
NQO1	NAD(P)H Quinone Dehydrogenase 1
ACSL4	Acyl-CoA Synthetase Long Chain Family Member 4
FTH1	Ferritin Heavy Chain 1
TF	Transferrin
ChIP assay	Chromatin immunoprecipitation (ChIP) assay

and bile acid levels and is highly expressed in the liver, intestine, and kidneys, especially the renal proximal tubular epithelial cells [16]. In kidney diseases, FXR is reported to exhibit anti-lipogenic, anti-inflammatory, antifibrotic, and antioxidant activities. Previous studies have demonstrated that the pharmacological activation of FXR alleviates oxidative stress, upregulates antioxidant genes, and restores aberrant glutathione (GSH) metabolism [15,17]. We have previously demonstrated that FXR deficiency increases lipid peroxide accumulation, HMOX1 expression, and apoptosis *in vivo* and in cells [13]. These findings suggest that FXR may mediate apoptosis and other types of cell death.

Recent studies have examined NR-mediated regulation of ferroptosis [18,19]. However, the underlying mechanisms involved in ferroptosis regulation have not been elucidated. This study examined the crucial role of FXR in ferroptosis using a mouse model of cisplatin-induced AKI. Pharmacological activation of FXR mitigated cisplatin-induced oxidative stress and ferroptosis in cells and mice. Genomic analysis revealed that FXR directly or indirectly regulates the transcription of ferroptosis-associated genes through the FXR or FXR-MAFG pathway.

2. Materials and methods

2.1. Materials

Anti-FXR (sc-13063), anti-ACSL4 (sc-365230), anti-FTH1 (sc-376594), and anti-GAPDH (sc-32233) antibodies were purchased from Santa Cruz Biotechnology (Dallas, TX, USA), while anti-HMOX1 (43966), anti-caspase8 (4790), anti-caspase3 (9662), anti-cleaved caspase3 (9661), anti-actin (4970), and anti-3-nitro tyrosine (3-NT) (9691) antibodies were purchased from Cell Signaling (Danvers, MA, USA). Anti-MAFG (PA5-30086) and anti-4-hydroxynonenal (4HNE) (bs-6313R) antibodies were purchased from Invitrogen (Carlsbad, CA, USA) and Bioss (Woburn, MA, USA), respectively. Anti-AIFM2 (LS-C382008-50) antibody was purchased from LSBio (Seattle, WA, USA). GW4064 was obtained from Tocris Bioscience (Bristol, UK). Anti-GPX4 antibody (ab219592) was obtained from Abcam (Cambridge, UK). Erastin was purchased from MedChemExpress. Ferrostatin-1 and cisplatin were purchased from Sigma, Inc (St. Louis, MO, USA). The Image-iT lipid peroxidation kit (C11-BODIPY 581/591) was purchased from Thermo Fisher (Waltham, MA, USA). ON-TARGETplus human short-interfering RNAs against FXR (siFXR, L-003414) and AIFM2(siAIFM2, L-004443) were purchased from Dharmacon, Inc (Lafayette, CO, USA).

2.2. Animal experiments

Eight-week-old male Male C57BL6 and global FXR knockout (KO) mice (JAX stock #004144) were purchased from Samtako (Korea) and Jackson Laboratory (Bar Harbor, ME, USA), respectively. Mice were intraperitoneally injected with vehicle (physiological saline) or cisplatin (20 mg/kg bodyweight in sterile physiological saline) through a single injection. GW4064 (30 mg/kg bodyweight) was administered to mice through oral gavage once a day for four consecutive days before and after cisplatin administration. Mice were sacrificed at 48 or 72 h post-cisplatin treatment. Serum and renal tissue samples of mice were collected. Blood urea nitrogen (BUN) and serum creatinine (sCr) levels were analyzed. All animal experiments were approved by the Animal Care Regulations Committee of Chonnam National University Medical School (CNUHIACUC-22002) and were performed according to the institutional guidelines for experimental animal care and use.

2.3. Cell culture

Human renal proximal tubular epithelial cells (HK2 cells) purchased from the American Type Culture Collection (Manassas, VA, USA) were cultured in Dulbecco's modified Eagle's medium-F-12 (WelGene, Daegu, Korea) supplemented with 10% fetal bovine serum, 100 U/mL penicillin, and 100 μg/mL streptomycin at 37 °C in a humidified atmosphere containing 5% CO_2. For cisplatin treatment, cells starved for one day in serum-free medium, were treated with cisplatin (10 μM) and GW4064 (1 μM) for the indicated duration in the same medium in all experiments.

2.4. Microscopy experiments

To perform immunofluorescence analysis, HK2 cells were incubated with 2 μM C11-BODIPY 581/591 (Image-iT™ lipid peroxidation kit C10445, Thermo Fisher), a lipid peroxidation sensor, for 20 min at 37 °C and subsequently, counterstained with Hoechst 33258. Then, the medium was removed, and the cells were washed three times with phosphate-buffered saline (PBS). Cells were imaged through confocal microscopy using filters for Hoechst (blue, nuclei), FITC (green, for oxidized lipid), and Texas Red (red, for non-oxidized lipid) channels.

2.5. siRNA transfection

The expression of FXR and AIFM2 was silenced using ON-TARGETplus siRNA from Dharmacon. Briefly, cells were transfected with 30 nM siFXR or siAIFM2 using DharmaFECT 1 transfection reagent, following the manufacturer's instructions. Control cells were transfected with control siRNA (siControl; ON-TARGETplus Non-Targeting Pool).

2.6. Western blotting analysis

To prepare cell lysates, the cell pellets were sonicated in radioimmunoprecipitation assay (RIPA) buffer (50 mM Tris-HCl (pH 7.6), 150 mM NaCl, 5 mM ethylenediaminetetraacetic acid, 1% NP40, 0.1% sodium dodecyl sulfate, and protease inhibitors). Similarly, the renal tissues were also homogenized in RIPA buffer. Cell and tissue lysates were centrifuged at 15,000 *g* and 4 °C for 10 min to remove cell debris. Immunoblotting was performed, as described previously [13], to detect target proteins using the indicated antibodies. The protein band

intensities were quantified using ImageJ software (National Institutes of Health, Bethesda, MD, USA).

2.7. Histological analysis

The renal tissues were fixed with 4% paraformaldehyde in phosphate-buffered saline (PBS) and embedded in paraffin. The paraffin-embedded sections were subjected to immunohistochemistry (IHC) and hematoxylin and eosin (H&E) staining. IHC was performed using the indicated antibodies and horseradish peroxidase-conjugated anti-mouse or anti-rabbit IgG secondary antibodies (Dako). The stained sections were imaged using the Nikon Eclipse Ni–U microscope (Tokyo, Japan). The staining intensities were quantified using ImageJ software (National Institutes of Health).

2.8. Quantification of mRNA

Total RNA was extracted from the mice renal tissues and HK2 cells using TRIzol reagent (Invitrogen). The extracted RNA (1 μg) was reverse-transcribed into complementary DNA (cDNA) using the avian myeloblastosis virus reverse transcription system (Promega Corp., Madison, WI, USA). Quantitative real-time polymerase chain reaction (qRT-PCR) was performed using SyGreen Blue Mix Hi-ROX (PCRBIO-SYSTEMS, London, UK) and StepOnePlus Real-Time PCR System (Thermo Fisher Scientific). The primers used in qRT-PCR are listed in Supplementary Table 1.

2.9. Terminal deoxynucleotidyl transferase dUTP nick-end labeling (TUNEL) assay

Apoptosis was determined using the ApopTag Plus peroxidase *in situ* apoptosis detection kit (Chemicon International; Temecula, CA, USA) or DeadEnd™ fluorometric TUNEL system (Promega Corporation) for *in vivo* experiments, following the manufacturer's instructions. The sections were counterstained with methyl green and examined under a light microscope.

2.10. Chromatin immunoprecipitation (ChIP) assay

ChIP assay was performed using a previously described method with minor modifications [20]. Briefly, the renal tissues were finely minced and incubated with 1% formaldehyde in PBS for 12 min, followed by incubation with glycine to quench formaldehyde. Cells were resuspended in hypotonic buffer and homogenized. Nuclei were pelleted and sonicated using Sonics VCX130. The samples were centrifuged to obtain the chromatin fraction. Subsequently, the chromatin fraction was precleared and immunoprecipitated using 1 μg of indicated antibody or IgG (control) overnight at 4 °C. Immunoprecipitation was performed with ZymoMag Protein A. The beads were washed, and the chromatin was purified using the Zymo Spin ChIP kit (Zymo Research, Irvine, CA, USA), following the manufacturer's instructions. qRT-PCR was performed to examine the expression levels of FXR or MAFG by comparing the threshold cycle (Ct) value of input DNA. The binding sequences of FXR or MAFG in the target genes were determined using the ChIP-sequencing data from the UCSC database (http://genome.ucsc.edu/) and GSM2053719, respectively [21,22]. Primer sequences are listed in Supplementary Table 2.

2.11. RNA sequencing

RNA was isolated from the renal tissues of mice using TRIzol reagent (Invitrogen), following the manufacturer's instructions and sent to Macrogen (Macrogen Incorporated, Korea) for library preparation and sequencing. A library was independently prepared with total RNA (1 μg/sample) using the Illumina TruSeq stranded total RNA sample prep kit (Illumina, Inc., San Diego, CA, USA). The RNA was purified, fragmented, and primed for cDNA synthesis. The cleaved RNA fragments were reverse-transcribed into first-strand cDNA using reverse transcriptase and random hexamers. Next, second-strand cDNA synthesis was performed using DNA polymerase I, RNase H, and dUTP. Next, the cDNA fragments were subjected to end repair process. A single 'A' base was added to the cDNA fragments, and the adapters were ligated. The products were purified and PCR-amplified to obtain the final cDNA library. The libraries were quantified using qRT-PCR according to the qPCR Quantification Protocol Guide (KAPA Library Quantification kits for Illumina Sequencing platforms). The quality of the libraries was determined using the TapeStation D1000 ScreenTape (Agilent Technologies, Waldbronn, Germany). The libraries were sequenced on the Illumina NovaSeq 6000 platform. The sequencing data have been deposited in the Gene Expression Omnibus (GEO) database of National Center for Biotechnology Information [23] with a GEO Series accession number GSE193860 (https://www.ncbi.nlm.nih.gov/geo/query/acc.cgi?acc=GSE193860).

2.12. Measurement of malondialdehyde (MDA), iron, and GSH/GSH disulfide (GSSG) ratio

The lipid peroxide content in the cells and tissues was determined using the EZ-lipid peroxidation (TBARS) assay kit (TBA200, Dogen) using MDA as a standard. The iron levels in cells and renal tissues were determined using the iron colorimetric assay kit (K390-100, Biovision), following the manufacturer's instructions. The GSH/GSSG ratio in cells and renal tissues was determined using the GSH/GSSG ratio detection assay kit (ab205811, Abcam), following the manufacturer's instructions.

2.13. Statistical analysis

All statistical analyses were performed using GraphPad Prism 8 software, version 8.01 (GraphPad Software, Inc San Diego, CA, USA). The mean values between groups were compared using one-way or two-way analysis of variance (ANOVA) with Bonferroni post hoc test for single or multiple comparisons. Differences were considered significant at $P < 0.05$. All experiments were performed at least three times.

3. Results

3.1. Cisplatin-induced AKI increases lipid peroxidation and decreases the expression of FXR and GPX4

The expression pattern of FXR was examined in a mouse model of cisplatin-induced AKI. The serum and renal tissue samples were collected from mice at 48 and 72 h post-cisplatin administration. The samples collected from saline-treated mice served as controls. The levels of BUN and sCr in the cisplatin-treated group were significantly increased when compared to those in the control group (Fig. 1A). Cisplatin administration time-dependently increased the levels of BUN and sCr. The levels of GPX4 (the central regulator of ferroptosis) and FXR were markedly decreased, while the levels of HMOX1 levels were markedly increased in mice with cisplatin-induced AKI (Fig. 1B). To examine the tissue morphology and lipid peroxidation, the renal tissues of control mice and mice with cisplatin-induced AKI were subjected to H&E, periodic acid-Schiff (PAS), 3-NT, and 4-HNE staining. Cisplatin time-dependently promoted tubular damage. The tubular epithelial cells were detached from the basement membrane, and the deposition of collagen was higher in the cisplatin-treated group compared to that in the control group. The levels of 3-NT and 4-HNE in the cisplatin-treated group were higher than that in the control group. This indicated that cisplatin promoted aberrant lipid peroxidation (Fig. 1C). These results suggest that cisplatin promotes lipid peroxidation and downregulates the expression of FXR and GPX4.

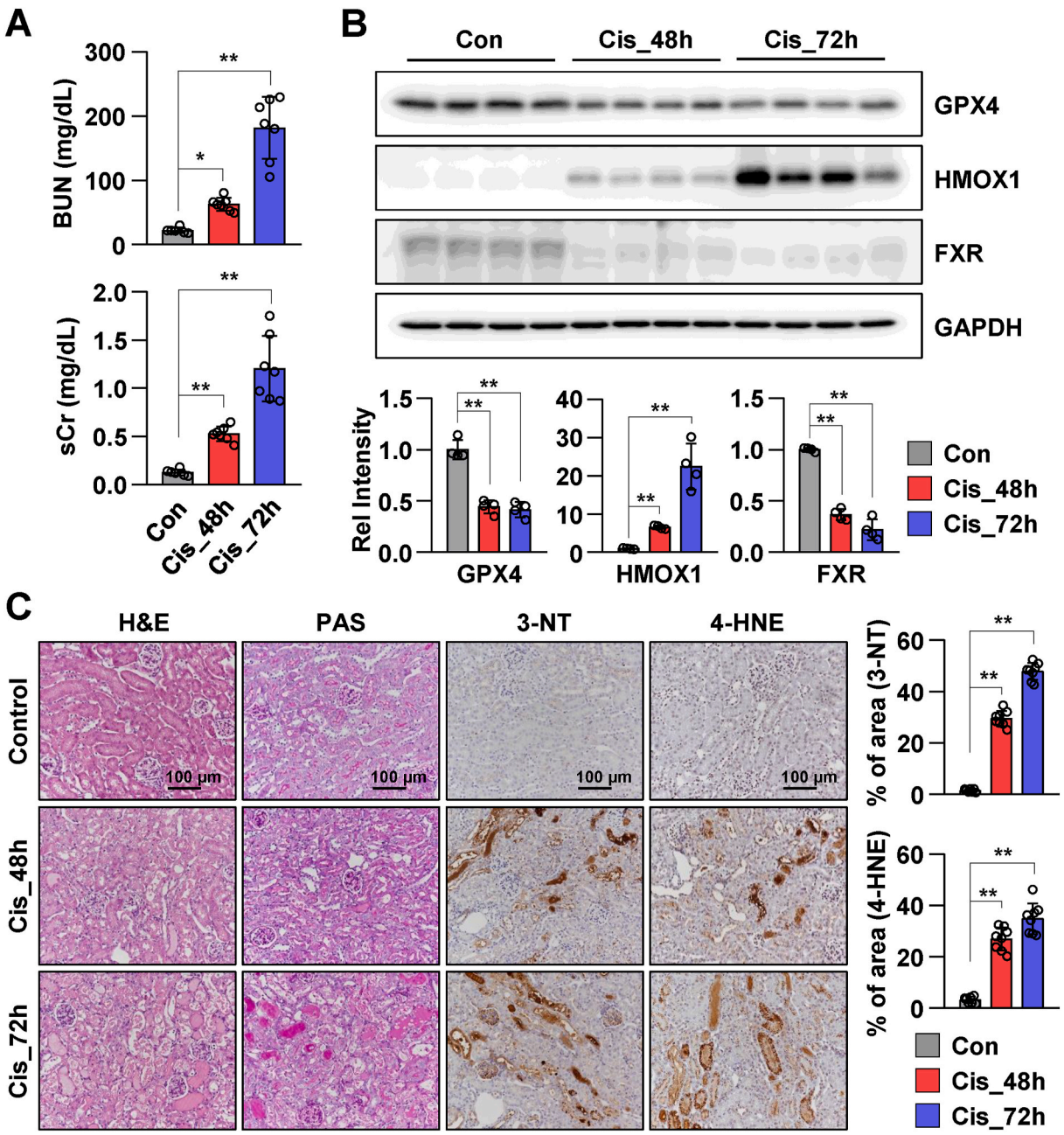

Fig. 1. Cisplatin promotes renal ferroptosis and downregulates FXR expression in mice.
The serum and the kidneys were collected from mice after 48 h and 72 h of cisplatin injection (20 mg/kg), (n = 6–7). (A) Serum BUN and Cr levels of each group. (B) Protein levels of GPX4, HMOX1, and FXR were detected by immunoblotting. The relative protein levels are shown. The values for the control group were set to 1. (C) Representative images of hematoxylin and eosin (H&E) and periodic acid-Schiff (PAS) staining to examine the histology and immunohistochemistry to examine the expression of 3-NT and 4-HNE. Scale bar, 100 μm. Computer-based morphometric analysis is shown (right bar graph, n = 7–8 in each group). All values are presented as the mean ± SD. Statistical significance was measured using one-way ANOVA with Bonferroni post hoc-test. *P < 0.05, **P < 0.005.

3.2. FXR deficiency increases renal lipid peroxidation and ferroptosis

Next, the role of FXR in the induction of lipid peroxidation and ferroptosis was examined using FXR knockdown HK2 cells and FXR KO mice. BUN and sCr levels in FXR KO mice were significantly increased when compared to those in wild-type (WT) mice. Malondialdehyde (MDA, a marker of lipid peroxidation) and iron levels were significantly increased, and the GSH/GSH disulfide (GSH/GSSG) ratio was decreased in FXR KO mice compared to those in the WT mice (Fig. 2A). Additionally, the levels of HMOX1, ACSL4, and FTH1 were markedly increased, and GPX4 levels were decreased in FXR KO mice compared to those in WT mice (Fig. 2B and Supplementary Fig. 1A). The levels of 3-NT and 4-HNE as well as cell death in FXR KO mice were increased when compared to those in WT mice (Fig. 2C). To examine whether FXR downregulation induces ferroptosis and lipid peroxidation, HK2 cells were transfected with siFXR. The levels of GPX4 were markedly decreased and HMOX1 levels were markedly increased in siFXR-transfected HK2 cells compared to those in siControl-transfected HK2 cells (Supplementary Fig. 1B). Next, siControl-transfected and siFXR-transfected HK2 cells were stained with C11-BODIPY 581/591 to examine lipid peroxidation. Lipid peroxidation in siFXR-transfected HK2 cells was increased compared to that in siControl-transfected HK2 cells (Supplementary Fig. 1C). These results suggest that FXR deficiency induces ferroptotic responses *in vivo* and *in vitro*.

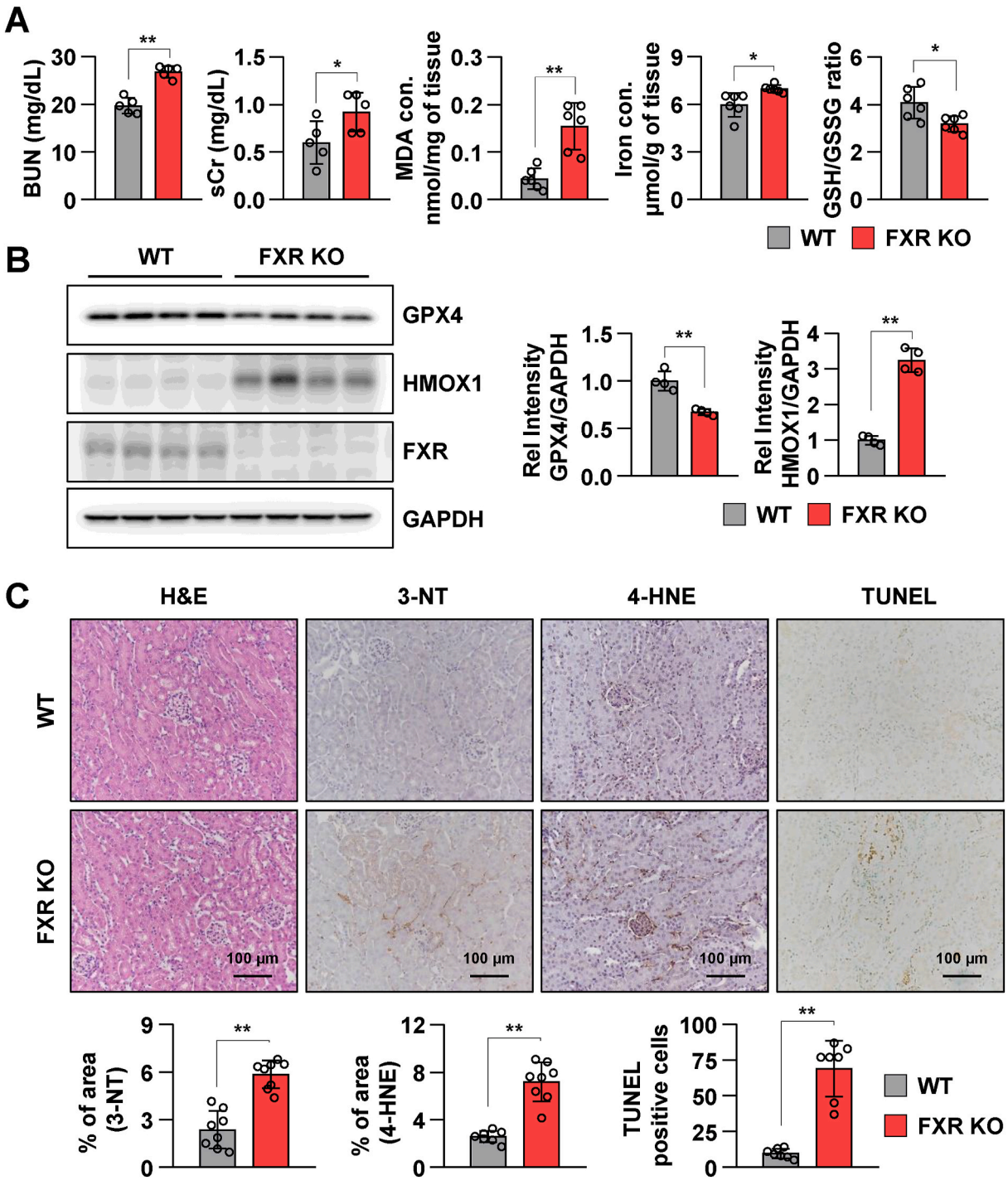

Fig. 2. FXR deficiency promotes renal injury and ferroptotic responses in mice.
The serum and kidney tissues were collected from wild-type (WT) and FXR knockout (FXR KO) mice (n = 6). (A) Serum BUN and Cr levels of each group. Malondialdehyde (MDA) and iron levels as well as GSH/GSSG ratio in kidney tissues. (B) Protein levels of GPX4, HMOX1, and FXR were detected by immunoblotting. The relative protein levels are shown. The values for the WT group were set to 1. (C) Representative images of hematoxylin and eosin (H&E) staining to examine the histology and immunohistochemistry to examine the expression of 3-NT and 4-HNE. Computer-based morphometric analysis is shown (bar graph, n = 8 in each group). Representative image of TUNEL staining. Quantitative analysis of positive TUNEL staining is shown (n = 7). Scale bar, 100 μm. All values are presented as the mean ± SD. Statistical significance was measured using one-way ANOVA with Bonferroni post hoc-test. *P < 0.05, **P < 0.005.

3.3. *Pharmacological activation of FXR inhibits ferroptosis in HK2 cells*

Next, the effect of cisplatin in FXR knockdown HK2 cells was examined. Compared to those in vehicle-treated siControl-transfected HK2 cells, MDA and iron levels were increased and the GSH/GSSG ratio was decreased in cisplatin-treated siControl-transfected HK2 cells. The changes in the levels of MDA and iron as well as GSH/GSSG ratio were significantly pronounced in cisplatin-treated siFXR-transfected HK2 cells (Fig. 3A). Cisplatin-induced decrease in GPX4 levels in siFXR-transfected HK2 cells was higher than that in siControl-transfected HK2 cells. Additionally, the increase in HMOX1 levels in cisplatin-treated siControl-transfected HK2 cells was higher than that in

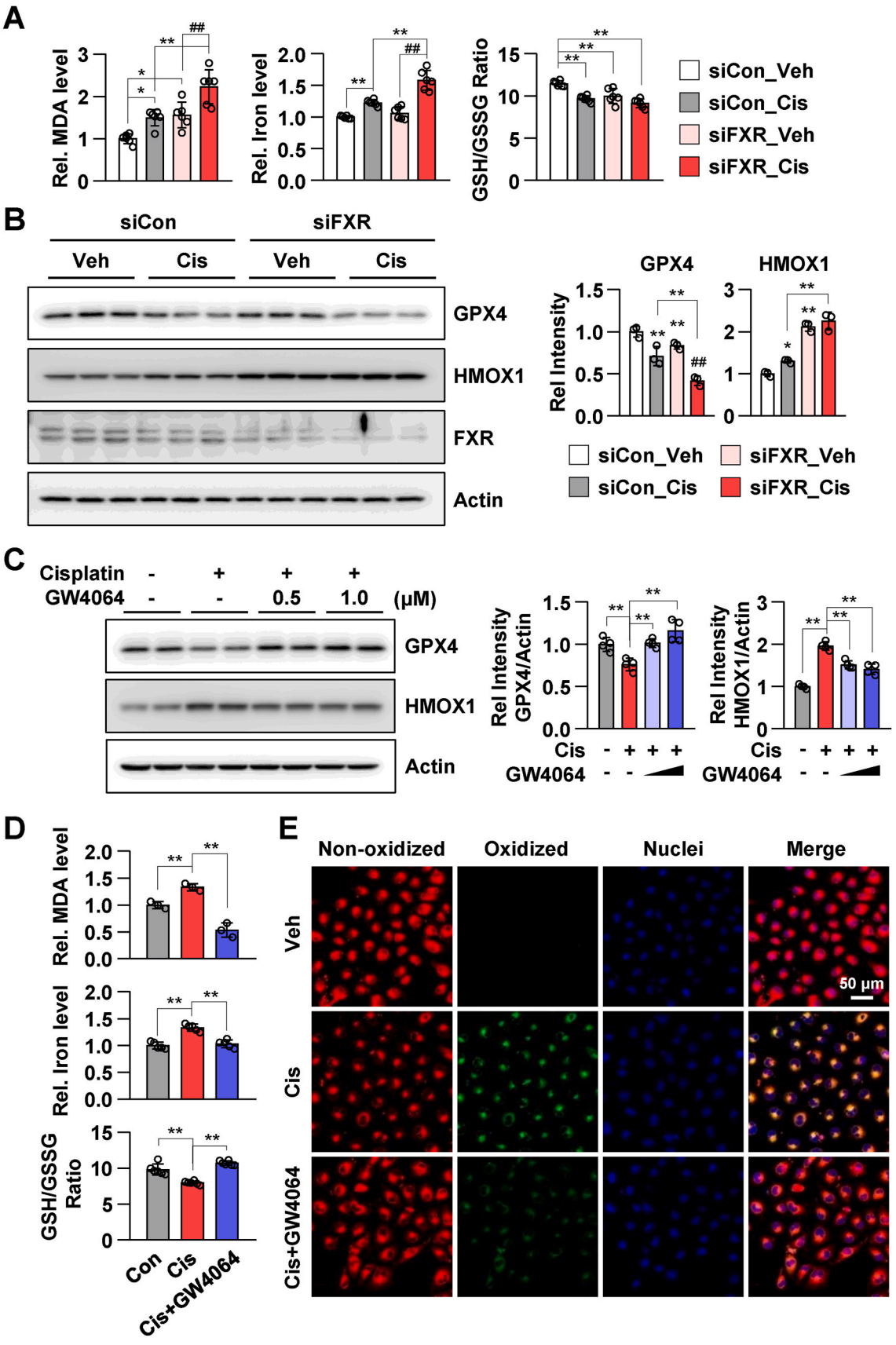

(caption on next page)

Fig. 3. FXR agonist GW4064 mitigates cisplatin-induced ferroptotic responses in HK2 cells.
(A) HK2 cells were transfected with siControl or siFXR as indicated; 48 h later, the cells were treated with cisplatin (10 μM) for 24 h. The levels of MDA and iron, and GSH/GSSG ratio in HK2 cells (n = 6). (B) Protein levels of GPX4, HMOX1, and FXR were detected by immunoblotting. The relative protein levels are shown. The values for vehicle-treated siControl group were set to 1 (n = 3). (C–E) After treatment with GW4064 (1 μM) for 2 h, HK2 cells were treated with cisplatin (10 μM) for another 24 h. (C) Protein levels of GPX4 and HMOX1 were detected by immunoblotting. The relative protein levels are shown. The values for the vehicle group were set to 1 (n = 4). (D) The relative levels of MDA and iron as well as GSH/GSSG ratio are shown. (E) After treatment with cisplatin and GW4064, the cells were incubated with C11-BODIPY 581/591 (2 μM) and Hoechst 33258 for counterstaining; the images were then immediately visualized by confocal microscopy. Confocal microscopy showed non-oxidized lipid (red, Texas Red) and oxidized lipid (green, FITC). scale bar, 50 μm. All values are presented as the mean ± SD. Statistical significance was measured using one- or two-way ANOVA with Bonferroni post hoc-test. *P < 0.05, **P < 0.005. (For interpretation of the references to color in this figure legend, the reader is referred to the Web version of this article.)

vehicle-treated siFXR-transfected and cisplatin-treated siFXR-transfected HK2 cells (Fig. 3B). Next, the effect of the FXR agonist GW4064 on the regulation of ferroptosis was examined. Treatment with GW4064 mitigated cisplatin-induced decreases in GPX4 and increases in HMOX1 expression levels (Fig. 3C). Additionally, treatment with GW4064 mitigated cisplatin-induced increases in MDA and iron levels and decreases in the GSH/GSSG ratio in HK2 cells (Fig. 3D). Consistent with these results, GW4064 mitigated cisplatin-induced increases in lipid peroxidation in live HK2 cells (Fig. 3E). These results suggest that pharmacological activation of FXR inhibited cisplatin-induced ferroptosis.

3.4. Activation of FXR negatively regulates erastin-induced ferroptosis

Next, we examined the suppressive effects of pharmacological FXR activation on the effects of erastin, which induces ferroptosis by inhibiting cystine/glutamate antiporter (xCT) and glutathione synthesis [24]. Treatment with ferrostatin-1 (Fer-1, ferroptosis inhibitor) and GW4064 mitigated erastin-induced decrease in of GPX4 expression in HK2 cells (Fig. 4A). Additionally, treatment with Fer-1 and GW4064 mitigated erastin-induced increase in MDA and iron levels and decrease in the GSH/GSSG ratio (Fig. 4B). Consistent with these results, Fer-1 and GW4064 mitigated erastin-induced increase in lipid peroxidation in live HK2 cells (Fig. 4C). These data indicated that GW4064-activated FXR inhibits ferroptosis.

3.5. FXR activation alleviates renal ferroptosis in a mouse model of cisplatin-induced AKI

The inhibitory effects of GW4064 on ferroptosis in a mouse model of cisplatin-induced AKI were examined. WT mice were administered with GW4064 through oral gavage, followed by cisplatin, as shown in the schematic diagram (Fig. 5A). Treatment with GW4064 significantly mitigated cisplatin-induced increase in the levels of BUN, sCr, neutrophil gelatinase-associated lipocalin (NGAL), MDA, and iron and decrease in the GSH/GSSG ratio in mice with AKI (Fig. 5B). Immunoblotting was performed to examine the expression levels of ferroptosis-associated proteins, such as GPX4, HMOX1, ACSL4, and FTH1. Treatment with GW4064 mitigated cisplatin-induced decrease in GPX4 and increase in HMOX1, ACSL4, and FTH1 expression in mice with AKI (Fig. 5C). Since cisplatin has been reported to induce apoptotic cell death, the levels of apoptotic markers, including caspase 8 and caspase 3 in the AKI mouse model were examined. Treatment with GW4064 mitigated cisplatin-induced increase in caspase 8 and cleaved-Casp3/Casp3 ratio (Supplementary Fig. 2). Consistently, GW4064 mitigated cisplatin-induced changes in the mRNA levels of ferroptosis-related genes, such as *Gpx4*, *Hmox1*, *Acsl4*, *Gstp1*, *Gstp2*, *Gsta3*, and *Ggt6* (Fig. 5D). Histological changes in the renal section were analyzed using H&E, PAS, 3-NT, and 4-HNE staining. H&E and PAS staining revealed that GW4064 mitigated cisplatin-induced degeneration of tubular epithelium with loss and swelling of brush borders. IHC analysis revealed that GW4064 significantly mitigated cisplatin-induced increase in the production of reactive oxygen species (ROS) and lipid damage (Fig. 5E). These results indicated that GW4064-activated FXR inhibited ferroptosis in a mouse model of cisplatin-induced AKI.

3.6. FXR deficiency exacerbates renal ferroptosis in a mouse model of cisplatin-induced AKI

Next, renal ferroptosis in FXR KO mice was examined. After 48 h cisplatin treatment, the levels of BUN, sCr, NGAL, MDA, and iron were increased compared to those in vehicle-treated WT mice, and the GSH/GSSG ratio was decreased in cisplatin-treated WT mice. Furthermore, the levels of BUN, sCr, NGAL, MDA, and iron were markedly increased, and the GSH/GSSG ratio was markedly decreased in cisplatin-treated FXR KO mice compared to those in WT mice (Fig. 6A). Immunoblotting was performed to examine the expression levels of ferroptosis-associated proteins, including GPX4, HMOX1, ACSL4, and FTH1. Decreased GPX4 levels and increased HMOX1, ACSL4, and FTH1 levels in cisplatin-treated WT mice were further exacerbated in cisplatin-treated FXR KO mice (Fig. 6B). Consistent with these results, cisplatin-induced changes in the mRNA levels of ferroptosis-related genes, such as *Gpx4*, *Hmox1*, *Acsl4*, *Gstp1*, *Gstp2*, *Gsta3*, and *Ggt6* in WT mice were further exacerbated in cisplatin-treated FXR KO mice (Fig. 6C). H&E, PAS, 3-NT, and 4-HNE staining revealed that cisplatin-treated mice exhibited increased renal tubulointerstitial damage and elevated levels of ROS generation and lipid damage. Compared to those in WT mice, renal damage, ROS levels, and lipid damage were higher in cisplatin-treated FXR KO mice (Fig. 6D). These results suggest that FXR deficiency promotes renal ferroptosis and renal damage and that FXR is important to protect against renal ferroptosis.

3.7. FXR regulates ferroptosis-related genes in mouse kidneys

To investigate the function of renal FXR, renal tissues of WT and FXR KO mice, treated with vehicle or GW4064, were subjected to RNA sequencing (Fig. 7A). The expression levels of 72 and 146 genes were significantly downregulated and upregulated, respectively, in GW4064-treated WT mice compared to those in vehicle-treated WT mice (over 1.5-fold change) (Fig. 7B). Gene ontology (GO) and Kyoto Encyclopedia of Genes and Genomes (KEGG) analyses revealed that the significantly upregulated genes were involved in lipid metabolic, bile acid transmembrane transporter, and glutathione metabolic processes. Furthermore, the significantly downregulated genes were involved in cell death, adipocytokine signaling, and bile secretion (Fig. 7C and Supplementary Fig. 3A). The expression levels of organic solute transporter-encoding genes (*Slc51a* and *Slc51b*), direct FXR target genes (*Osgin1* and *Mafg*), glutathione metabolism-related genes (*Gsta4* and *Ggt6*), ferroptosis-related gene (*Aifm2*), and lipid metabolism-related genes (*Amacr*, *Dgkd*, *Plin5*, and *Tysnd1*) were upregulated, whereas the expression levels of ROS response-related genes (*Hmox1*, *Cryab*, and *Nqo1*) and lipid metabolism-related genes (*Aldh1a3*, *Acox2*, *Lpin1*, *Acnat2*, and *Cyp4a14*) were downregulated upon treatment with GW4064 (Fig. 7D). Consistent with the RNA-seq data, qRT-PCR analysis revealed that GW4064 treatment significantly upregulated the mRNA levels of *Slc51a*, *Slc51b*, *Osgin1*, *Mafg*, *Gsta4*, *Ggt6*, *Aifm2*, *Amacr*, *Dgkd*, *Plin5*, and *Tysnd1* and downregulated the mRNA levels of *Hmox1*, *Cryab*, *Aldh1a3*, *Acox2*, *Lpin1*, *Acnat2*, *Nqo1*, and *Cyp4a14* in the renal tissues of WT mice (Fig. 7E). The expression levels of 88 and 144 genes were significantly downregulated and upregulated, respectively, in vehicle-treated FXR KO mice compared to those in the vehicle-treated WT mice (Supplementary

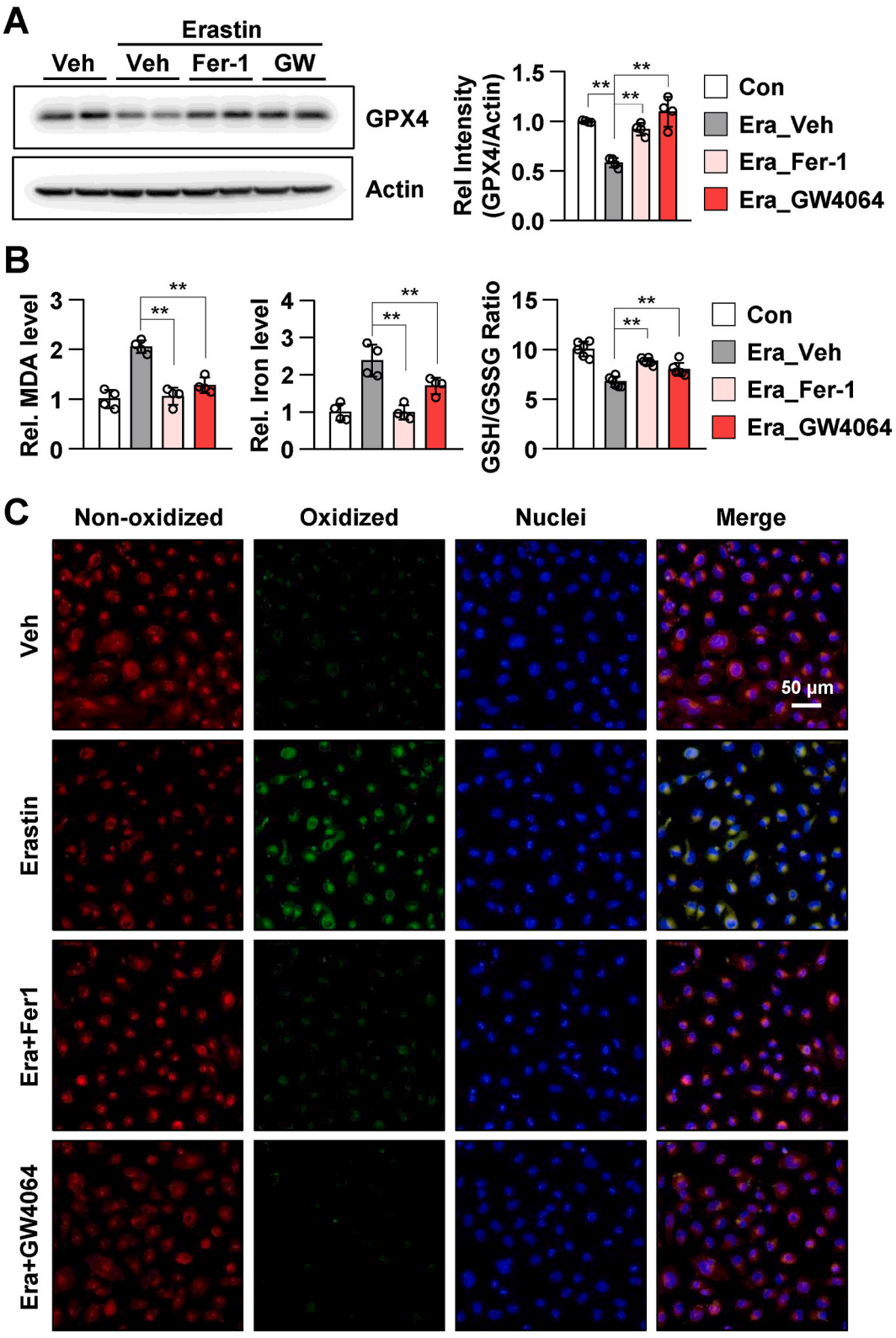

Fig. 4. FXR agonist GW4064 mitigates erastin-induced ferroptotic responses in HK2 cells.
After treatment with ferrostatin-1 (Fer-1, 5 μM) and GW4064 (1 μM) for 2 h, HK2 cells were treated with erastin (5 μM) for another 24 h. (A) Protein levels of GPX4 were detected by immunoblotting. The relative protein levels are shown. The values for the vehicle group were set to 1 (n = 4). (B) The relative levels of MDA and iron and GSH/GSSG ratio are shown. (C) After treatment with Fer-1 and GW4064, the cells were incubated with C11-BODIPY 581/591 (2 μM) and Hoechst 33258 for counterstaining; the images were then immediately visualized by confocal microscopy. Confocal microscopy showed non-oxidized lipid (red, Texas Red) and oxidized lipid (green, FITC). scale bar, 50 μm. All values are presented as the mean ± SD. Statistical significance was measured using one- or two-way ANOVA with Bonferroni post hoc-test. **P < 0.005. (For interpretation of the references to color in this figure legend, the reader is referred to the Web version of this article.)

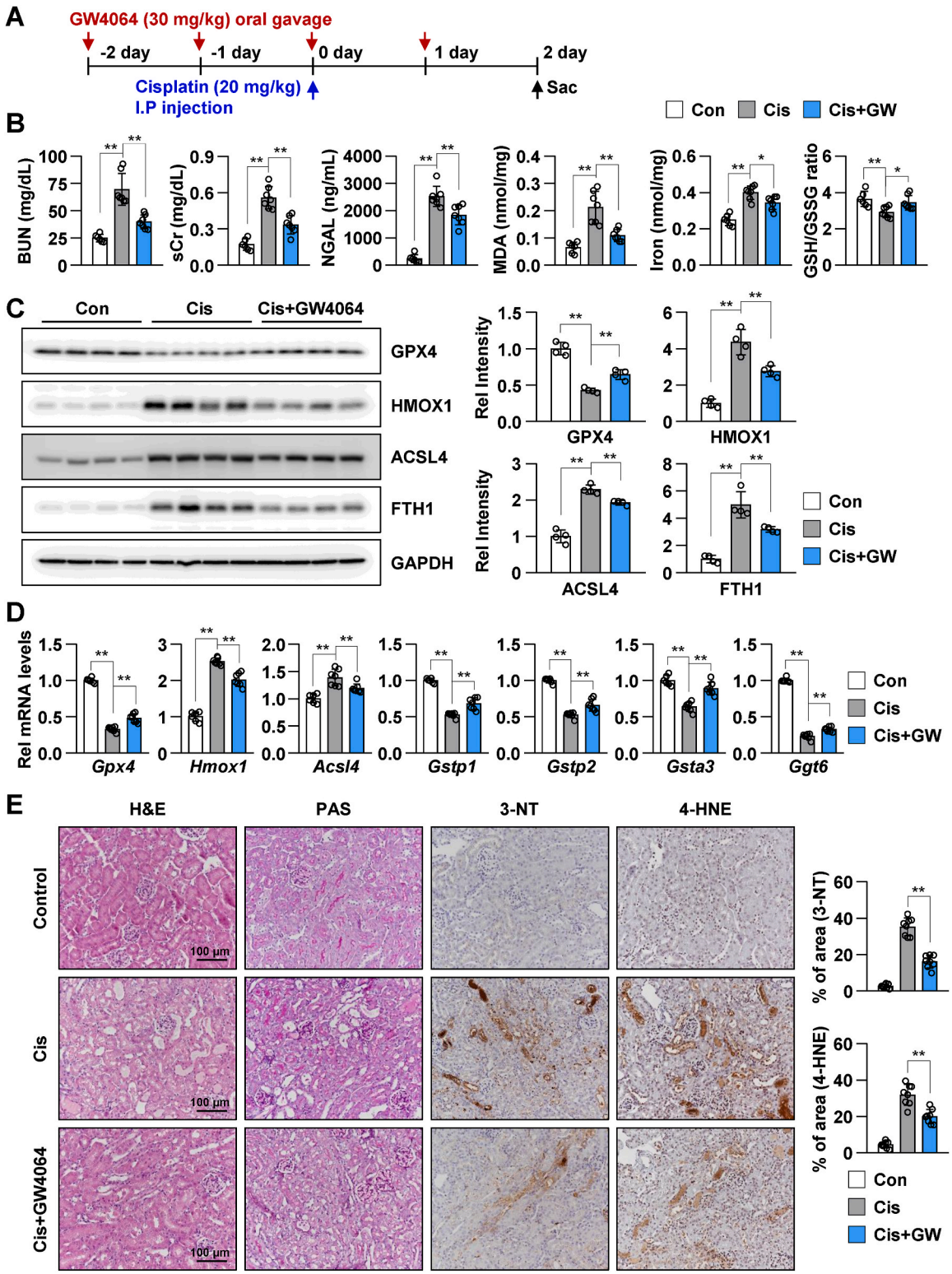

Fig. 5. FXR activation mitigates cisplatin-induced renal injury and ferroptotic response in a mouse model of cisplatin-induced AKI.
WT mice were administered with GW4064 or vehicle (soybean oil) by oral gavage (single daily administration for 4 days) as shown in the experimental outline (A). The mice were injected with cisplatin (20 mg/kg) on the third day of GW4064 administration. After 48 h of cisplatin injection, the serum and the kidneys were collected. (B) BUN, sCr, and neutrophil gelatinase-associated lipocalin (NGAL) levels were measured in the serum. MDA, iron levels, and GSH/GSSG ratio were measured in the kidney tissue (n = 6–7). (C) Protein levels of GPX4, HMOX1, ACSL4, and FTH1 were detected by immunoblotting. The relative protein levels are shown. The values for the control group were set to 1 (n = 4). (D) The mRNA levels of the indicated genes were measured by qRT-PCR. The values for control group are set to 1. (E) Representative images of H&E and PAS staining to examine histology. Paraffin-embedded kidney tissue sections were stained with antibodies against 3-NT and 4-HNE (scale bar 100 μm). Computer-based morphometric analysis is shown (right bar graph, n = 8 in each group). All values are presented as the mean ± SD. Statistical significance was measured using one-way ANOVA with Bonferroni post hoc-test. *P < 0.05, **P < 0.005.

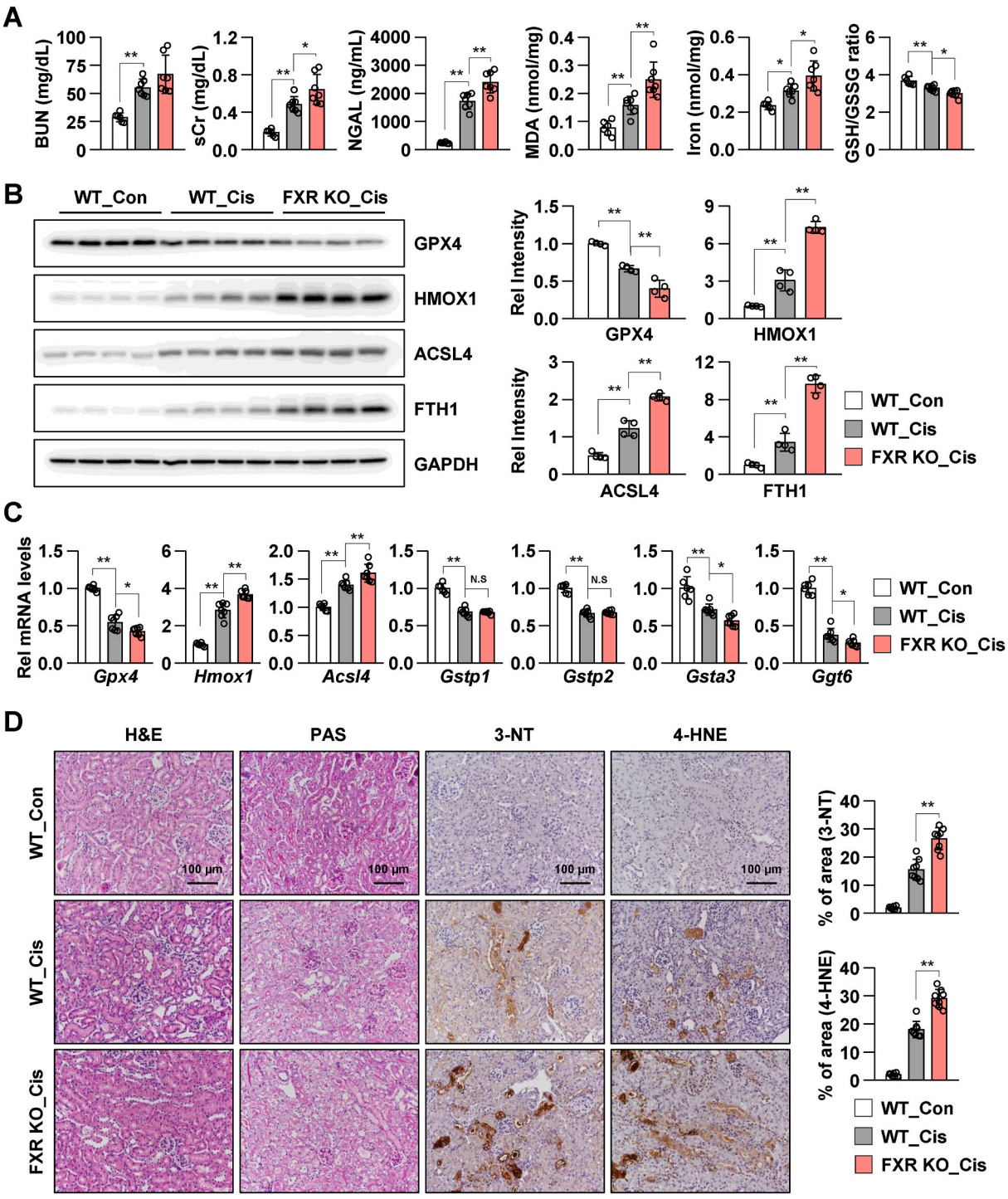

Fig. 6. FXR deficiency exacerbates cisplatin-induced renal injury and ferroptotic response in a mouse model of the AKI.
The WT and FXR knockout mice were intraperitoneally injected with cisplatin (20 mg/kg) or vehicle control (saline). After 48 h of cisplatin injection, the serum and the kidneys were collected. (A) BUN, sCr, and neutrophil gelatinase-associated lipocalin (NGAL) levels were measured in the serum. MDA and iron levels and GSH/GSSG ratio were measured in the kidney tissue (n = 6–7). (B) Protein levels of GPX4, HMOX1, ACSL4, and FTH1 were detected by immunoblotting. The relative protein levels are shown. The values for the WT control group were set to 1 (n = 4). (C) The mRNA levels of the indicated genes were measured by qRT-PCR. The values for the control group are set to 1. (D) Representative images of H&E and PAS staining to examine histology. Paraffin-embedded kidney tissue sections were stained with antibodies against 3-NT and 4-HNE (scale bar 100 μm). Computer-based morphometric analysis is shown (right bar graph, n = 7–8 in each group). All values are presented as the mean ± SD. Statistical significance was measured using one-way ANOVA with Bonferroni post hoc-test. *P < 0.05, **P < 0.005.

Fig. 3B). GO and KEGG analyses revealed that the significantly upregulated genes were enriched in fatty acid metabolic process and peroxisome and cholesterol metabolism (Supplementary Figs. 3C and D). qRT-PCR analysis revealed that FXR deficiency significantly upregulated the mRNA levels of fatty acid metabolic process-associated genes (*Acox1*, *Plin2*, *Acsl1*, *Acsl4*, *Cyp4a12a*, *Cyp4a12b*, and *Cyp4a14*) (Supplementary Figs. 3E and F). The results of RNA-seq analysis suggest that FXR plays an important role in the transcriptional activation of ferroptosis and lipid peroxisome in the kidney.

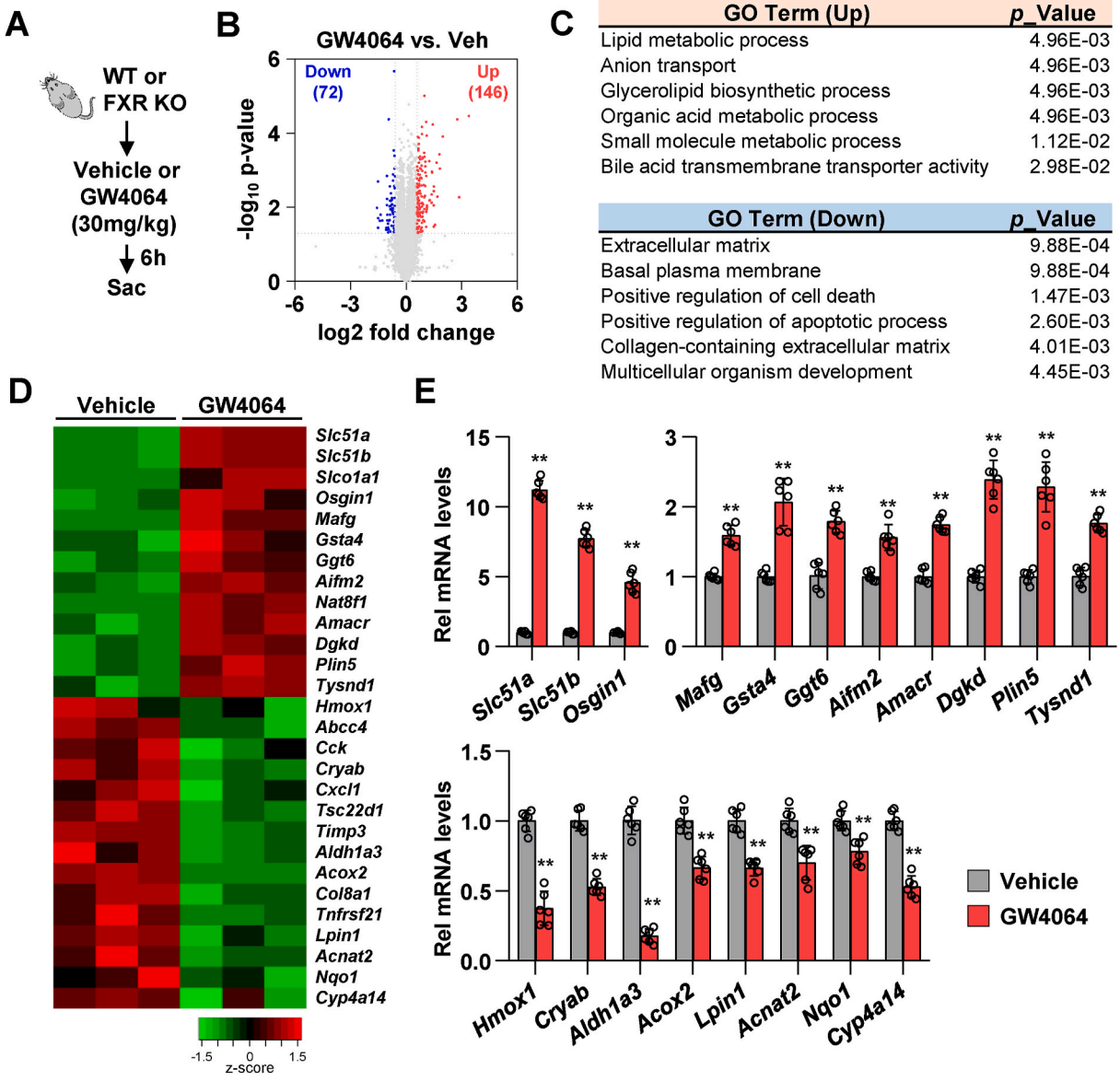

Fig. 7. FXR activation upregulates the expression of lipid and glutathione metabolism-related genes.
WT and FXR KO mice were fasted for 16 h and were subsequently administered GW4064 or vehicle (soybean oil) by oral gavage. After 6 h of GW4064 administration, the kidneys were collected. (A) Experimental outline. (B–D) RNA-sequencing analysis: (B) Volcano plots of RNA-seq data obtained using WT mice kidney tissues treated with vehicle or GW4064 (30 mg/kg). Blue, down-regulated genes; red, up-regulated genes. (C) Gene ontology (GO) analysis of genes either up- or down-regulated. (D) Heat maps showing changes in gene expression in WT mice treated with GW4064 compared to WT mice treated with vehicle. (E) The mRNA levels of the selected genes were measured by qRT-PCR (n = 6). The values for vehicle-treated group are set to 1. All values are presented as the mean ± SD. Statistical significance was measured using one-way ANOVA with Bonferroni post hoc-test. **P < 0.005. (For interpretation of the references to color in this figure legend, the reader is referred to the Web version of this article.)

3.8. Agonist-activated FXR binds to the DNA of ferroptosis-related genes

FXR is a member of the NR superfamily of ligand-activated transcription factors. Hence, the regulatory effects of FXR on the transcription of ferroptosis-related genes were examined. The DNA-binding sites of FXR in the direct target genes of FXR (*Slc51a*, *Slc51b*, *Osgin1*, and *Mafg*) and ferroptosis-related genes (*Aifm2*, *Ggt6*, and *Gsta4*) were analyzed from the published liver and intestine chromatin immunoprecipitation-sequencing (ChIP-seq) data (Supplementary Fig. 4A) [22]. We examined whether FXR binds to its DNA-binding site in these genes after GW4064 treatment in mouse renal tissues as described in Fig. 8A. The ChIP assay revealed that treatment with GW4064 increased the occupancy of FXR to its binding sites in *Slc51a*, *Slc51b*, *Osgin1*, and *Mafg*. Similarly, the occupancy of FXR to its binding sites in ferroptosis-associated genes (*Aifm2*, *Ggt6*, and *Gsta4*) in GW4064-treated mouse renal tissues was significantly higher than that in vehicle-treated mouse renal tissues (Fig. 8B). In particular, treatment with GW4064 significantly upregulated the mRNA expression level of *Aifm2*, which was recently reported to suppress phospholipid peroxidation and ferroptosis [25,26], in WT mice but not in FXR KO mice (Supplementary Fig. 4B). Treatment with GW4064 significantly upregulated *Aifm2* mRNA levels in cisplatin-induced AKI mouse model (Supplementary Fig. 4C). Furthermore, to test whether *Aifm2*, a ferroptosis-related direct target gene of FXR, has a protective effect on cisplatin-induced HK2 cells, we used siRNA and an inhibitor of AIFM2 in cisplatin-treated HK2 cells. Upon treatment with cisplatin, a decrease in GPX4 protein levels and increase in MDA levels were more pronounced in siAIFM2-transfected and iFSP1 (an inhibitor of AIFM2)-treated HK2

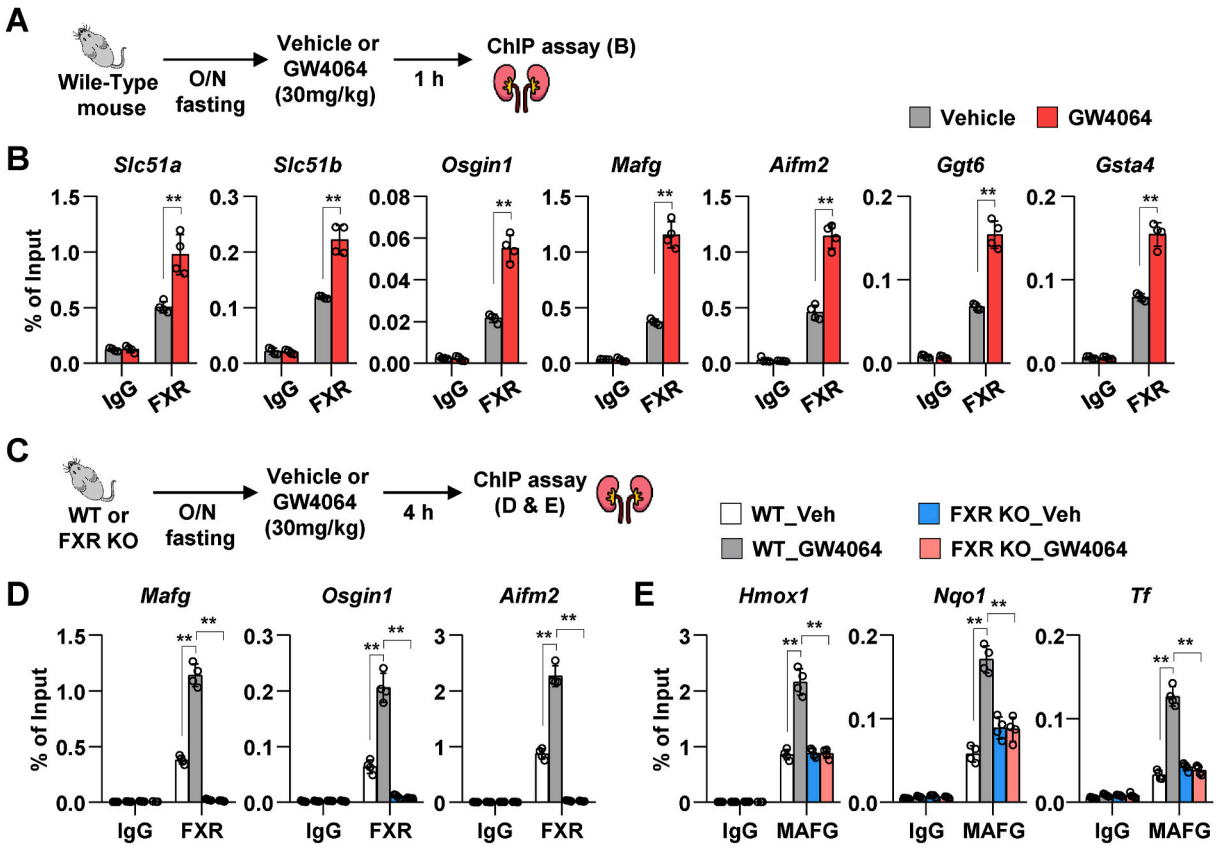

Fig. 8. FXR epigenetically activates ferroptosis-related genes.
WT and FXR KO mice were fasted overnight (16 h) and were subsequently administered GW4064 or vehicle by oral gavage. After 1 h or 4 h of GW4064 administration, ChIP assay was performed using mice kidney tissues. (A and C) Experimental outline. (B) ChIP assay was performed after treatment with GW4064 for 1 h. Occupancy of FXR at the indicated genes (n = 4 mice). (D–E) ChIP assay was performed after treatment with GW4064 for 4 h. Occupancy of FXR (D) and MAFG (E) at the indicated genes (n = 4 mice). All values are presented as the mean ± SD. Statistical significance was measured using one- or two-way ANOVA with Bonferroni post hoc-test. *P < 0.05, **P < 0.005.

cells than in siControl-transfected and vehicle-treated HK2 cells, respectively (Supplementary Fig. 5). However, GPX4 protein levels and MDA levels did not change in vehicle-treated HK2 cells in both siAIFM2 transfected group and iFSP1-treated group compared to those in the control group. Consistent with these results, cisplatin treatment-induced increase in lipid peroxidation in siAIFM2-transfected HK2 cells was further increased when compared to that in siControl-transfected HK2 cells (Supplementary Fig. 5C).

Furthermore, *Mafg*, a target gene of FXR, has been reported to be a transcriptional repressor [21]. Hence, the transcriptional repressive effects of MAFG on ferroptosis-related genes were examined. ChIP assay was performed using renal tissues of WT and FXR KO mice. Treatment with GW4064 for 4 h markedly increased MAFG levels in WT mice but not in FXR KO mice (Supplementary Fig. 6A). The DNA-binding sites of MAFG in ROS response-related (*Hmox1* and *Nqo1*) and ferroptosis-related (*Transferrin* [*Tf*]) genes were analyzed using the published liver ChIP-seq data (Supplementary Fig. 6B) [21]. Additionally, the effect of GW4064 on the binding of MAFG to these genes in mouse renal tissues was examined (Fig. 8C). ChIP assay revealed that treatment with GW4064 promoted the occupancy of FXR to its binding sites in *Mafg*, *Osgin1*, and *Aifm2* in the renal tissues of WT mice but not in the renal tissues of FXR KO mice (Fig. 8D). Additionally, treatment with GW4064 for 4 h promoted the occupancy of MAFG to its binding sites in *Hmox1*, *Nqo1*, and *Tf* in WT mice but not in FXR KO mice (Fig. 8E). The findings of protein/DNA interaction studies suggest that pharmacologically-activated FXR in mouse renal tissues directly or indirectly regulates the transcription of ROS response-related and ferroptosis-related genes and that the activation of MAFG is dependent on FXR.

4. Discussion

This study demonstrated that FXR regulates lipid peroxidation and ferroptosis and that it exerts protective effects against cisplatin-induced AKI in mice. In addition, it was shown that FXR directly or indirectly regulates the transcription of ferroptosis-related genes through the FXR or FXR-MAFG pathway.

Cisplatin-induced AKI is associated with cell death processes, including apoptosis, necrosis, and autophagy [27–29]. Cisplatin reacts rapidly with thiol-containing antioxidant molecules such as glutathione and is converted to a highly reactive form, and when glutathione is depleted, intracellular oxidative stress increases [30]. Additionally, cisplatin increases renal iron levels in rats and mice and promotes iron-catalyzed oxidative damage, which accelerates renal ferroptosis [31–33]. Previous studies have demonstrated that inhibition of ferroptosis by modulating MIOX expression, repurposing drugs and hormones as anti-ferroptosis agents, and activating vitamin D receptor and Ras homolog enriched in brain (Rheb1) signaling exerts renal protective effects in experimental models of cisplatin-induced AKI [18,34–36]. In this study, GPX4 (ferroptosis marker) and FXR levels were decreased and lipid peroxide levels were increased in a mouse model of cisplatin-induced AKI. We have previously demonstrated that FXR deficiency increases HMOX1 expression and lipid peroxidation levels in both mice and cells [13]. Additionally, this study demonstrated that FXR deficiency decreases GPX4 expression levels and GSH/GSSG ratio and increases iron and lipid peroxidation levels. HMOX1 is a well-known

antioxidant enzyme. However, sustained high expression or excessive activation of HMOX1 alters iron homeostasis and induces ferroptosis in various cell types [37,38]. High expression of HMOX1 due to FXR deficiency may fail to regulate iron homeostasis, leading to ferroptosis. This suggested that FXR may be important for the regulation of the renal ferroptotic pathway.

Previous studies have reported that FXR exerts renal protective effects in various diseases, such as obesity, diabetic nephropathy, kidney I/R injury, and unilateral ureteral obstruction [11,12,14,39]. Additionally, FXR has been reported to exert protective effects in cisplatin-induced renal injury [40]. However, the correlation between FXR and ferroptosis regulation has not been examined. In this study, treatment with GW4064 mitigated cisplatin-induced changes in GPX4 and HMOX1 expression levels, lipid peroxidation, iron content, and GSH/GSSG ratio in HK2 cells. Additionally, the anti-ferroptotic effect of FXR was demonstrated using HK2 cells treated with erastin, a ferroptosis activator. Treatment with GW4064 mitigated cisplatin-induced changes in the levels of ferroptosis markers in WT mice with AKI. In contrast, cisplatin-induced ferroptotic phenotypes and kidney injuries were exacerbated in FXR KO mice. Cisplatin is reported to induce renal apoptosis. In this study, treatment with GW4064 mitigated cisplatin-induced increase in Casp8 expression as well as cleaved-Casp3/Casp3 ratio in the renal tissues of WT mice. While the inhibitory effect of FXR on renal oxidative stress has been shown in a previous report [41,42], we found that pharmacological activation of FXR decreases the levels of lipid peroxidase and iron content, as well as ameliorates ferroptotic phenotypes in both mice and cells. These results suggest that FXR may be a key regulatory component of the apoptotic and ferroptotic pathways.

RNA-seq and ChIP assay data strongly support the role of FXR in ferroptosis regulation. Treatment with GW4064 upregulated the expression of direct target genes of FXR involved in bile secretion and transcriptional repression, including *Slc51a*, *Slc51b*, and *Mafg* but downregulated the expression of ROS response-related genes, including *Hmox1* and *Cryab*. Additionally, renal mRNA levels of *Acsl4*, associated with ferroptosis and peroxisome metabolism, in FXR KO mice were upregulated when compared to those in WT mice. Furthermore, mechanistic studies suggested that FXR is important for the regulation of the transcriptional activity of its target genes as well as ferroptosis-related genes.

This study demonstrated that *Aifm2* (Apoptosis Inducing Factor Mitochondria Associated 2), which is known to prevent lipid oxidative damage and ferroptosis by catalyzing the reduction of coenzyme Q/ubiquinone-10 to ubiquinol-10 in the plasma membrane [43], is a novel target gene of FXR. Recently, Doll et al. and Bersuker et al. identified a gene encoding FSP1 (Ferroptosis Suppressor Protein 1, also called AIFM2) [25,26]. Ferroptosis, an iron-dependent pathway, induces cell death by promoting lipid peroxidation in the membrane. Cell membrane damage during ferroptosis can be prevented by GPX4 and GSH. Doll et al. and Bersuker et al. demonstrated that ferroptosis can be inhibited by AIFM2 (FSP1) even in the absence of GPX4. Consistent with these previous studies, in our data, downregulation of AIFM2, either by siRNA or by treatment with iFSP1 inhibitor, in cisplatin-treated HK2 cells decreased GPX4 expression and further increased lipid peroxidation compared to those in the cisplatin-treated control group. RNA-sequencing results revealed that the mRNA levels of *Aifm2* were increased in GW4064-treated WT mice compared to those in the vehicle-treated group. In addition, through ChIP-seq data analysis, we found that FXR binds to DNA sequences, called FXR response elements (FXREs), such as IR1 (inverted repeat1), IR8 (inverted repeat8), and ER8 (eight nucleotides), on the *Aifm2* gene. This study demonstrated that *Aifm2* is a novel target gene of FXR and its transcription is regulated by FXR. However, further studies are needed to examine the role of modulating AIFM2 expression in renal diseases.

The MAF family is divided into small MAF proteins (sMAFs) (MAFG, MAFF, and MAFK) and large MAF proteins (cMAF, MAFA, and MAFB) [44]. sMAFs are basic region leucine zipper (bZIP) type transcription factors that lack a transcriptional activation domain, and their homodimers act as transcriptional repressors [45]. Vallim et al. demonstrated that *Mafg* is a direct target gene of FXR and that it is a repressor of bile acid homeostasis-related genes by ChIP-sequencing and microarray analysis of mouse liver [21]. Consistently, this study showed that the mRNA and protein expression levels of MAFG were increased in an FXR-dependent manner *in vivo*. Based on the ChIP-seq data [21], the DNA-binding site of MAFG in ROS response-related and ferroptosis-related genes was analyzed. ChIP analysis of the renal tissues of WT and FXR KO mice revealed that MAFG regulates the transcription of *Hmox1*, *Nqo1*, and *Tf* through an FXR-dependent mechanism. MAFG forms a heterodimer with NRF2 and regulates the genes involved in stress response and detoxification [46]. Future studies are needed to elucidate the correlation between the MAFG-NRF2 heterodimer and FXR.

This study demonstrated the renal protective effect of FXR from cell death by ferroptosis in a mouse model of cisplatin-induced AKI. Pharmacological activation of FXR attenuated ferroptosis and lipid peroxidation in both mice and human cells. Notably, FXR directly or indirectly regulated the transcription of ferroptosis-associated genes through the FXR or FXR-MAFG pathway. These findings suggest a novel mechanistic role of FXR in the regulation of ferroptosis, which can be a potential therapeutic target for renal injury to mitigate renal cell death programs in AKI.

Author contributions

D.H.K. and S.W.K. designed the study; D.H.K., H.I.C., and J.S.P. carried out experiments; D.H.K., H.I.C., J.S.P., C.S.K., E.H.B., S.K.M., and S.W.K. analyzed the data; and D.H.K. and S.W.K. wrote the paper.

Ethics statement

All animal experiments were approved by the Ethics Committee of Chonnam National University Medical School.

Funding statement

This research was supported by Basic Science Research Program through the National Research Foundation of Korea (NRF) funded by the Ministry of Education (2019R1I1A3A01051599), by the National Research Foundation of Korea funded by the Korea government (MSIT) (2019R1A2C2086276, 2020R1A2C1003310, and 2022R1A2C1004852).

Declaration of competing interest

The authors declare that they have no conflict of interest.

Acknowledgments

We appreciate the supports of our experimenters.

Appendix A. Supplementary data

Supplementary data to this article can be found online at https://doi.org/10.1016/j.redox.2022.102382.

References

[1] A. Khwaja, KDIGO clinical practice guidelines for acute kidney injury, Nephron Clin. Pract. 120 (2012) c179–184, https://doi.org/10.1159/000339789.
[2] N.H. Lameire, A. Bagga, D. Cruz, J. De Maeseneer, Z. Endre, J.A. Kellum, et al., Acute kidney injury: an increasing global concern, Lancet 382 (2013) 170–179, https://doi.org/10.1016/S0140-6736(13)60647-9.

[3] R.P. Miller, R.K. Tadagavadi, G. Ramesh, W.B. Reeves, Mechanisms of cisplatin nephrotoxicity, Toxins (Basel) 2 (2010) 2490–2518, https://doi.org/10.3390/toxins2112490.

[4] S. Sears, L. Siskind, Potential therapeutic targets for cisplatin-induced kidney injury: lessons from other models of AKI and fibrosis, J. Am. Soc. Nephrol. (2021), https://doi.org/10.1681/ASN.2020101455.

[5] A. Ozkok, C.L. Edelstein, Pathophysiology of cisplatin-induced acute kidney injury, BioMed Res. Int. 967826 (2014), https://doi.org/10.1155/2014/967826, 2014.

[6] S.J. Dixon, K.M. Lemberg, M.R. Lamprecht, R. Skouta, E.M. Zaitsev, C.E. Gleason, et al., Ferroptosis: an iron-dependent form of nonapoptotic cell death, Cell 149 (2012) 1060–1072, https://doi.org/10.1016/j.cell.2012.03.042.

[7] J. Li, F. Cao, H.L. Yin, Z.J. Huang, Z.T. Lin, N. Mao, et al., Ferroptosis: past, present and future, Cell Death Dis. 11 (88) (2020), https://doi.org/10.1038/s41419-020-2298-2.

[8] B.R. Stockwell, J.P. Friedmann Angeli, H. Bayir, A.I. Bush, M. Conrad, S.J. Dixon, et al., Ferroptosis: a regulated cell death nexus linking metabolism, redox biology, and disease, Cell 171 (2017) 273–285, https://doi.org/10.1016/j.cell.2017.09.021.

[9] Y. Chen, H. Fan, S. Wang, G. Tang, C. Zhai, L. Shen, Ferroptosis: a novel therapeutic target for ischemia-reperfusion injury, Front. Cell Dev. Biol. 9 (2021), 688605, https://doi.org/10.3389/fcell.2021.688605.

[10] R.M. Evans, D.J. Mangelsdorf, Nuclear receptors, RXR, and the big bang, Cell 157 (2014) 255–266, https://doi.org/10.1016/j.cell.2014.03.012.

[11] T. Jiang, X.X. Wang, P. Scherzer, P. Wilson, J. Tallman, H. Takahashi, et al., Farnesoid X receptor modulates renal lipid metabolism, fibrosis, and diabetic nephropathy, Diabetes 56 (2007) 2485–2493, https://doi.org/10.2337/db06-1642.

[12] D.H. Kim, H.I. Choi, J.S. Park, C.S. Kim, E.H. Bae, S.K. Ma, et al., Src-mediated crosstalk between FXR and YAP protects against renal fibrosis, Faseb. J. 33 (2019) 11109–11122, https://doi.org/10.1096/fj.201900325R.

[13] D.H. Kim, J.S. Park, H.I. Choi, C.S. Kim, E.H. Bae, S.K. Ma, et al., The critical role of FXR is associated with the regulation of autophagy and apoptosis in the progression of AKI to CKD, Cell Death Dis. 12 (2021) 320, https://doi.org/10.1038/s41419-021-03620-z.

[14] X.X. Wang, T. Jiang, Y. Shen, Y. Caldas, S. Miyazaki-Anzai, H. Santamaria, et al., Diabetic nephropathy is accelerated by farnesoid X receptor deficiency and inhibited by farnesoid X receptor activation in a type 1 diabetes model, Diabetes 59 (2010) 2916–2927, https://doi.org/10.2337/db10-0019.

[15] X.X. Wang, D. Wang, Y. Luo, K. Myakala, E. Dobrinskikh, A.Z. Rosenberg, et al., FXR/TGR5 dual agonist prevents progression of nephropathy in diabetes and obesity, J. Am. Soc. Nephrol. 29 (2018) 118–137, https://doi.org/10.1681/ASN.2017020222.

[16] S. Modica, R.M. Gadaleta, A. Moschetta, Deciphering the nuclear bile acid receptor FXR paradigm, Nucl. Recept. Signal. 8 (2010), e005, https://doi.org/10.1621/nrs.08005.

[17] Z. Gai, T. Gui, C. Hiller, G.A. Kullak-Ublick, Farnesoid X receptor protects against kidney injury in uninephrectomized obese mice, J. Biol. Chem. 291 (2016) 2397–2411, https://doi.org/10.1074/jbc.M115.694323.

[18] Z. Hu, H. Zhang, B. Yi, S. Yang, J. Liu, J. Hu, et al., VDR activation attenuate cisplatin induced AKI by inhibiting ferroptosis, Cell Death Dis. 11 (73) (2020), https://doi.org/10.1038/s41419-020-2256-z.

[19] Y. Wang, Z. Wang, Z. Wu, M. Chen, D. Dong, P. Yu, et al., Involvement of REV-ERBalpha dysregulation and ferroptosis in aristolochic acid I-induced renal injury, Biochem. Pharmacol. 193 (2021), 114807, https://doi.org/10.1016/j.bcp.2021.114807.

[20] D.H. Kim, Z. Xiao, S. Kwon, X. Sun, D. Ryerson, D. Tkac, et al., A dysregulated acetyl/SUMO switch of FXR promotes hepatic inflammation in obesity, EMBO J. 34 (2015) 184–199, https://doi.org/10.15252/embj.201489527.

[21] T.Q. de Aguiar Vallim, E.J. Tarling, H. Ahn, L.R. Hagey, C.E. Romanoski, R.G. Lee, et al., MAFG is a transcriptional repressor of bile acid synthesis and metabolism, Cell Metabol. 21 (2015) 298–311, https://doi.org/10.1016/j.cmet.2015.01.007.

[22] A.M. Thomas, S.N. Hart, B. Kong, J. Fang, X.B. Zhong, G.L. Guo, Genome-wide tissue-specific farnesoid X receptor binding in mouse liver and intestine, Hepatology 51 (2010) 1410–1419, https://doi.org/10.1002/hep.23450.

[23] R. Edgar, M. Domrachev, A.E. Lash, Gene Expression Omnibus: NCBI gene expression and hybridization array data repository, Nucleic Acids Res. 30 (2002) 207–210, https://doi.org/10.1093/nar/30.1.207.

[24] S.J. Dixon, D.N. Patel, M. Welsch, R. Skouta, E.D. Lee, M. Hayano, et al., Pharmacological inhibition of cystine-glutamate exchange induces endoplasmic reticulum stress and ferroptosis, Elife 3 (2014), e02523, https://doi.org/10.7554/eLife.02523.

[25] K. Bersuker, J.M. Hendricks, Z. Li, L. Magtanong, B. Ford, P.H. Tang, et al., The CoQ oxidoreductase FSP1 acts parallel to GPX4 to inhibit ferroptosis, Nature 575 (2019) 688–692, https://doi.org/10.1038/s41586-019-1705-2.

[26] S. Doll, F.P. Freitas, R. Shah, M. Aldrovandi, M.C. da Silva, I. Ingold, et al., FSP1 is a glutathione-independent ferroptosis suppressor, Nature 575 (2019) 693–698, https://doi.org/10.1038/s41586-019-1707-0.

[27] W. Lieberthal, V. Triaca, J. Levine, Mechanisms of death induced by cisplatin in proximal tubular epithelial cells: apoptosis vs. necrosis, Am. J. Physiol. 270 (1996) F700–F708, https://doi.org/10.1152/ajprenal.1996.270.4.F700.

[28] Q. Wei, G. Dong, J. Franklin, Z. Dong, The pathological role of Bax in cisplatin nephrotoxicity, Kidney Int. 72 (2007) 53–62, https://doi.org/10.1038/sj.ki.5002256.

[29] C. Yang, V. Kaushal, S.V. Shah, G.P. Kaushal, Autophagy is associated with apoptosis in cisplatin injury to renal tubular epithelial cells, Am. J. Physiol. Ren. Physiol. 294 (2008) F777–F787, https://doi.org/10.1152/ajprenal.00590.2007.

[30] Z.H. Siddik, Cisplatin: mode of cytotoxic action and molecular basis of resistance, Oncogene 22 (2003) 7265–7279, https://doi.org/10.1038/sj.onc.1206933.

[31] R. Baliga, Z. Zhang, M. Baliga, N. Ueda, S.V. Shah, In vitro and in vivo evidence suggesting a role for iron in cisplatin-induced nephrotoxicity, Kidney Int. 53 (1998) 394–401, https://doi.org/10.1046/j.1523-1755.1998.00767.x.

[32] Y. Ikeda, H. Hamano, Y. Horinouchi, L. Miyamoto, T. Hirayama, H. Nagasawa, et al., Role of ferroptosis in cisplatin-induced acute nephrotoxicity in mice, J. Trace Elem. Med. Biol. 67 (2021), 126798, https://doi.org/10.1016/j.jtemb.2021.126798.

[33] S. Zhao, X. Wang, X. Zheng, X. Liang, Z. Wang, J. Zhang, et al., Iron deficiency exacerbates cisplatin- or rhabdomyolysis-induced acute kidney injury through promoting iron-catalyzed oxidative damage, Free Radic. Biol. Med. 173 (2021) 81–96, https://doi.org/10.1016/j.freeradbiomed.2021.07.025.

[34] F. Deng, I. Sharma, Y. Dai, M. Yang, Y.S. Kanwar, Myo-inositol oxygenase expression profile modulates pathogenic ferroptosis in the renal proximal tubule, J. Clin. Invest. 129 (2019) 5033–5049, https://doi.org/10.1172/JCI129903.

[35] Q. Lu, M. Wang, Y. Gui, Q. Hou, M. Gu, Y. Liang, et al., Rheb1 protects against cisplatin-induced tubular cell death and acute kidney injury via maintaining mitochondrial homeostasis, Cell Death Dis. 11 (2020) 364, https://doi.org/10.1038/s41419-020-2539-4.

[36] E. Mishima, E. Sato, J. Ito, K.I. Yamada, C. Suzuki, Y. Oikawa, et al., Drugs repurposed as antiferroptosis agents suppress organ damage, including AKI, by functioning as lipid peroxyl radical scavengers, J. Am. Soc. Nephrol. 31 (2020) 280–296, https://doi.org/10.1681/ASN.2019060570.

[37] B. Hassannia, B. Wiernicki, I. Ingold, F. Qu, S. Van Herck, Y.Y. Tyurina, et al., Nano-targeted induction of dual ferroptotic mechanisms eradicates high-risk neuroblastoma, J. Clin. Invest. 128 (2018) 3341–3355, https://doi.org/10.1172/JCI99032.

[38] C. Li, M.E. Lonn, X. Xu, G.J. Maghzal, D.M. Frazer, S.R. Thomas, et al., Sustained expression of heme oxygenase-1 alters iron homeostasis in nonerythroid cells, Free Radic. Biol. Med. 53 (2012) 366–374, https://doi.org/10.1016/j.freeradbiomed.2012.03.007.

[39] M. Huls, J.J. van den Heuvel, H.B. Dijkman, F.G. Russel, R. Masereeuw, ABC transporter expression profiling after ischemic reperfusion injury in mouse kidney, Kidney Int. 69 (2006) 2186–2193, https://doi.org/10.1038/sj.ki.5000407.

[40] E.H. Bae, H.S. Choi, S.Y. Joo, I.J. Kim, C.S. Kim, J.S. Choi, et al., Farnesoid X receptor ligand prevents cisplatin-induced kidney injury by enhancing small heterodimer partner, PLoS One 9 (2014), e86553, https://doi.org/10.1371/journal.pone.0086553.

[41] M. Nomoto, M. Miyata, S. Yin, Y. Kurata, M. Shimada, K. Yoshinari, et al., Bile acid-induced elevated oxidative stress in the absence of farnesoid X receptor, Biol. Pharm. Bull. 32 (2009) 172–178, https://doi.org/10.1248/bpb.32.172.

[42] Y.D. Wang, W.D. Chen, C. Li, C. Guo, Y. Li, H. Qi, et al., Farnesoid X receptor antagonizes JNK signaling pathway in liver carcinogenesis by activating SOD3, Mol. Endocrinol. 29 (2015) 322–331, https://doi.org/10.1210/me.2014-1225.

[43] B.R. Stockwell, A powerful cell-protection system prevents cell death by ferroptosis, Nature 575 (2019) 597–598, https://doi.org/10.1038/d41586-019-03145-8.

[44] F. Katsuoka, M. Yamamoto, Small maf proteins (MafF, MafG, MafK): history, structure and function, Gene 586 (2016) 197–205, https://doi.org/10.1016/j.gene.2016.03.058.

[45] H. Motohashi, F. Katsuoka, J.A. Shavit, J.D. Engel, M. Yamamoto, Positive or negative MARE-dependent transcriptional regulation is determined by the abundance of small Maf proteins, Cell 103 (2000) 865–875, https://doi.org/10.1016/s0092-8674(00)00190-2.

[46] M.B. Kannan, V. Solovieva, V. Blank, The small MAF transcription factors MAFF, MAFG and MAFK: current knowledge and perspectives, Biochim. Biophys. Acta (1823) 1841–1846, https://doi.org/10.1016/j.bbamcr.2012.06.012, 2012.